Peripheral nerve graft architecture affects regeneration

Vleggeert-Lankamp, Carmen Lia Anne-Marie

CHAPTER 5

Nerve graft porosity shortens the refractory period of regenerating nerve fibres

C.L.A.M. Vleggeert-Lankamp[a], J.F.C. Wolfs[a], A.P. Pêgo[b], R.J. van den Berg[c], H.K.P. Feirabend[a], M.J.A. Malessy[a], E.A.J.F. Lakke[a]

[a]Neuroregulation group, Department of Neurosurgery; [c]Department of Neurophysiology, Leiden University Medical Centre (LUMC), Leiden, the Netherlands; [b]Institute for Biomedical Technology (BMTI), Department of Polymer Chemistry and Biomaterials, University of Twente, Enschede, The Netherlands

Abstract

In the present study we consider the influence of porosity of synthetic nerve grafts on peripheral nerve regeneration. Microporous (1-10 µm) and non porous nerve grafts made of a copolymer of trimethylene carbonate (TMC) and poly-ε-caprolactone (CL) were tested. Twelve weeks after surgery, nerve and muscle morphological and electrophysiological results of regenerated nerves through the synthetic nerve grafts were compared to autografted and to unoperated sciatic nerves. Based on the observed changes of the number and diameter of the nerve fibres the predicted values of the electrophysiological parameters were calculated.

The values of the morphometrical parameters of the peroneal nerves and the gastrocnemic and tibial muscles were similar if not equal in the synthetic nerve grafted rats. The refractory periods however, were shorter in *porous* compared to *non porous* grafted nerves, and thus closer to unoperated values. A shorter refractory period enables the axon to follow the firing frequency of the neuron more effectively and allows a more adequate target organ stimulation. Therefore *porous* nerve grafts are preferred over *non porous* nerve grafts.

Introduction

The porosity of a synthetic nerve graft is one of the factors to consider in order to improve nerve regeneration. Favorable effects of permeability are attributed to inward diffusion of growth factors and extracellular matrix proteins [1], and to outward diffusion of waste products. Impermeable tubes, conversely, may have a positive effect on nerve regeneration because they insulate the area of axonal outgrowth, they prevent the invasion of connective tissue that leads to scarring, and growth factors generated inside the tube may be unable to diffuse away [2].

Literature data regarding porosity of synthetic nerve grafts are contradictory [2-8]. This is at least partially due to the fact that the quality of regeneration is determined from histological parameters. In a previous study we applied a broad array of evaluation methods, and we demonstrated that a combination of the evaluation of nerve and muscle morphology and in vivo electrophysiology could discern even subtle differences between *microporous* and *non porous* poly(ε-caprolactone)(CL) nerve grafts (chapter 4, this thesis). The outcome was very much in favour of the *microporous* nerve grafts mainly because the diameter of the tissue bridge crossing the nerve graft was much larger. It was concluded that porosity positively influenced the formation of a tissue bridge, and this was hypothesized to be the explanation of the beneficial effect of pores. However, in *microporous* CL nerve grafts, in 2 of 6 nerve grafts no tissue bridge could be demonstrated either. Apparently, the formation of a tissue bridge, which is a prerequisite for nerve regeneration, was problematical in a nerve graft of 100% ε-caprolactone. We demonstrated that the formation of a tissue bridge was not problematical in nerve grafts made of trimethylene carbonate (TMC) copolymerized with poly-ε-caprolactone (TMC/CL) (chapter 6, this thesis), because one of considerable size was present in all grafts. This motivated us to judge the influence of micropores in TMC/CL synthetic nerve grafts on newly regenerated axons again, this time with a presumed higher tissue bridge success ratio. Nerve guides with an outer layer of TMC/CL and an inner layer of either *non porous* TMC (*non porous* graft) or *porous* TMC (*porous* graft) were implanted in the rat sciatic nerve. Twelve weeks after bridging a 6 mm sciatic nerve lesion in the rat, the morphology of nerve at midgraft, morphometrical parameters of nerve and dependent muscle, and electrophysiological parameters of the nerve were evaluated. Based on the observed changes of the number and diameter of the regenerated nerve fibres predicted values of the electrophysiological parameters were calculated, to be compared to the actually measured values. The goal was to analyse whether the porosity of a synthetic nerve graft effects peripheral nerve regeneration, i.e. to assess the desirability of porosity.

Materials and methods

Synthetic nerve graft preparation

We implanted hollow synthetic nerve grafts consisting of two layers. The inner layer was fab - ricated by a dipcoating technique and consisted of *non porous* TMC (referred to as '*non porous* graft') or *porous* TMC (referred to as '*porous* graft'). To introduce micropores in the inner layer sugar crystals (<20 µm) were added, which were later allowed to leach out. The macroporous outer layer was nearly similar in both grafts and consisted of TMC/CL that was spun around the inner layer (fig. 1). The preparation of these tubes was comprehensively described in previ -

Figure 1: Synthetic nerve grafts

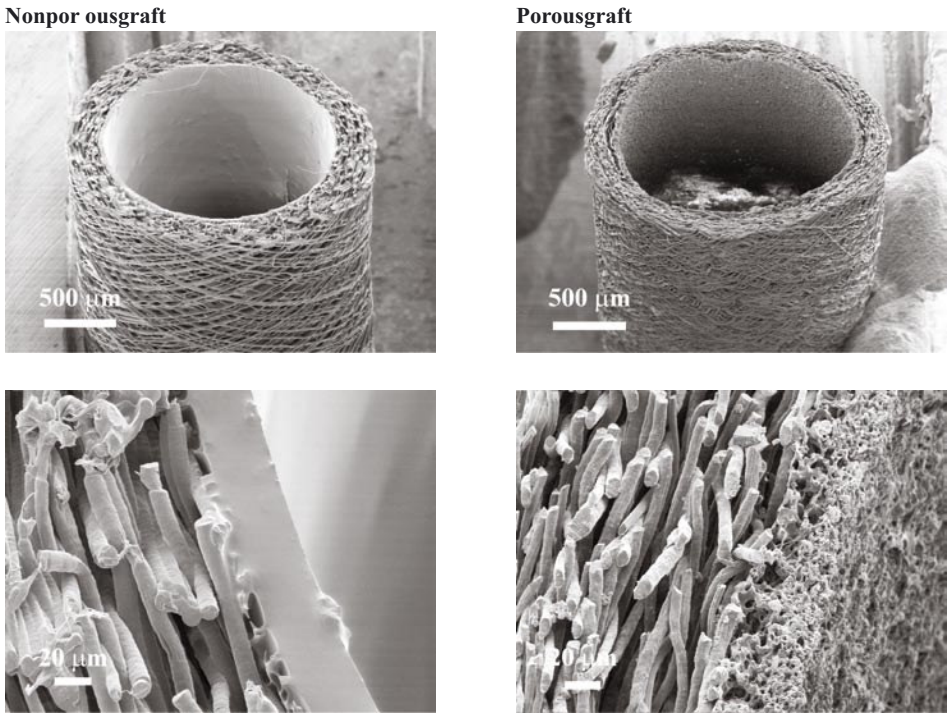

Scanning electron micrographs of cross-sections and details of the two-layer connections of synthetic nerve grafts. SEM analyses were carried out using a Hitachi S800 field emission scanning electron microscope at voltages of 3-5 kV [10].

Table 1: Characterization of synthetic tubes

	TMC/CL ratio in outer layer	**inner diameter** (mm)	**Wall thickness** (µm)		**Pore size** (µm)	
			inner layer	outer layer	inner layer	outer layer
Non porous graft	11 : 89	1.5	27	235	-	15-265
Porous graft	11 : 89	1.5	30	179	1-13	15-80

Internal diameter, wall thickness and porosities of the inner and outer layer of *non porous* and *porous* tubes, examined by scanning electron micrography (SEM).

ous studies [9, 10]. The physical properties of the resulting tubes were specified in table 1. All tubes had good flexing characteristics, and bending caused only a small reduction of the cross-sectional area of the tubal lumen.

In liquid nitrogen, tubes were cut into nerve grafts of 10 mm length. Prior to implantation, the nerve grafts were sterilized by rinsing them for 10 seconds in a 70 vol% ethanol solution, followed by a thorough rinse in sterilized water.

Animal model

A total of 30 female Wistar rats (HsdCpb:WU), weighing 220-240 grams, were used for this study. Rats were housed in flat bottomed cages in a central animal-care facility, and maintained on a 12-hour light cycle regime at a controlled temperature of 22°C. Standard rat chow and water were available *ad libitum*. Animals were randomly assigned to the control or to one of three sciatic nerve repair groups. Both sciatic nerves of 6 unoperated rats served as controls, 12 rats received an autograft, 6 rats received a *non porous* nerve graft, and 6 rats received a *porous* nerve graft. All grafting experiments were performed on the left sciatic nerve. Muscles reinnervated by an autografted nerve will be referred to as 'autograft muscles', and peroneal nerves distal to an autograft will be referred to as 'autograft peroneal nerves'. A similar nomenclature will be used for the muscles reinnervated by synthetic grafted nerves, and peroneal nerves distal to synthetic nerve grafts (for instance '*porous* graft muscle' and '*porous* graft peroneal nerve'). All experiments were performed in accordance with international and local laws governing the protection of animals used for experimental purposes (UDEC 99105).

Surgical procedures

For the grafting procedure, rats were given general inhalation anesthesia of isoflurane in a 1:1 mixture of O_2 and N_2O. To improve anesthesia and to diminish post-operative pain, buprenorphine (0.1 ml of 0.3 mg/ml; Temgesic®, Schering-Plough, Maarssen, the Netherlands) was injected intraperitoneally. Microsurgical dissection was performed with the aid of a Zeiss operating microscope under aseptic conditions. All animals were operated on in the same time span by the same surgeon. The left sciatic nerve was exposed and isolated at the midthigh level via a dorsal approach. In rats receiving an autograft, a 6 mm nerve segment was resected. The nerve segment (autograft) was reversed longitudinally and grafted into the gap with 4 epineurial sutures (10-0 monofilament nylon) at each end. In rats receiving a synthetic nerve graft, a 2 mm nerve segment was resected. The proximal and distal nerve stump were inserted into the synthetic nerve graft, leaving an interstump distance of 6 mm. Fibrin glue (Tissucol®, Baxter, Vienna, Austria) was used to affix the nerve stumps in the graft. The wound was closed in layers. After a post-operative survival period of 12 weeks, the rats were anaesthetized as described above, and the left sciatic nerve was exposed at the midthigh level via a dorsal approach. The (grafted) sciatic nerve was inspected, resected and stored in an electrolyte solution (140 mM NaCl, 3.0 mM KCl, 1.5 mM $CaCl_2$, 1.25 mM $MgSO_4$, and 11.0 mM glucose in 5.0 mM Tris buffer, pH 7.4, 20 °C). Immediately following resection of the sciatic

nerves, the gastrocnemic and anterior tibial muscles were exposed, resected, embedded in Tissuetek® (Sakura, Zoeterwoude, the Netherlands), rapidly frozen in liquid nitrogen cooled isopentane [11], and stored at -80°C. Finally the animals were euthanized.

Midgraft nerve morphological analysis

First, it was evaluated whether the nerve graft allowed tissue to bridge the gap between the nerve stumps. After the electrophysiological recordings were performed (see below), the nerve was stored in 4% formaldehyde solution (0.1 M phosphate buffered at pH 7.2) for at least a few weeks. Subsequently, 4 mm long samples were resected from the middle of the graft for microscopic inspection. Upon dehydration in ascending series of ethanol, the tissue samples were embedded in paraffin (Klinipath, Duiven, The Netherlands). Transverse 4 µm sections were cut and alternatingly stained for general appearance (haematoxylin/eosin), for myelin (Klüver-Barrera [12]), and for collagen (Verhoef van Gieson [13]).

Peroneal morphological analysis

Histology

The preparation of cross-sections of peroneal nerves and the subsequent microscopy and image analysis was comprehensively described in previous studies [14, 15]. In short, the nerves were immersion fixated and embedded in Epon® (Merck, Amsterdam, The Netherlands). Transverse 1 µm sections were stained with a 1% toluidine blue / 1% borax solution [16]. The nerve area, the mean nerve fibre diameter, the fibre density and the total number of nerve fibres were determined. Subsequently, the diameters of the nerve fibres were distributed into 180 classes of 0.1 µm each, and plotted against the percentage of the number of fibres present in that class. By fitting the sum of two lognormal functions to the frequency distributions of fibre diameters, the mean diameter and the number of fibres for the separate Aα- and Aβ-fibre populations were exposed. Fittings to two lognormal functions was compared to fittings with a single lognormal function using Akaike's Information Criterium (AIC).

Muscle morphological analysis

Immediately following the resection of the sciatic nerves, the gastrocnemic and anterior tibial muscles were exposed, resected, embedded, cut in 10 µm thick cross sections, and stained for myofibrillar ATPase. Microscopic video images of the sections were taken and the muscle cross sectional area (muscle CSA), the number of type I and type II muscle fibres, and the fibre cross sectional area of the type I and type II muscle fibres was determined as described elsewhere [15].

Electrophysiological evaluation

The in vitro electrophysiological evaluation of the sciatic nerve, including the peroneal and tibial nerve, was comprehensively described in a previous study [14]. In short, the resected

nerve was mounted on a moist chamber filled with an electrolyte solution (see above) in such a way that the grafted part was entirely floating in the middle pool. The nerve fibres were progressively recruited by extra-cellular excitation, while the propagated monophasic action potentials were measured and normalized in terms of compound action currents [14].

The presence *per se* of a measurable electrophysiological response was registered, and expressed as the *response rate*. When a response was present, then the displaced electrical charge was calculated (Q). Q_{max} was defined as the area under the curve of the maximum action current. The other parameters calculated were the mean conduction velocity (MCV), the mean voltage threshold (V_{50}), and the mean refractory period (t_{50}). When a measurable electrophysiological response was absent, Q_{max} was considered 0. As a consequence MCV, V_{50} and t_{50} remained undetermined.

In order to discriminate the Aα- and Aβ-fibre populations, two *erf*-functions were fitted to the stimulus-recruitment and interpulse time-recruitment curves [14]. Consequently values for $Q_{max,\alpha}$, $Q_{max,\beta}$ (calculated from stimulus-recruitment and interpulse time-recruitment curves separately), $V_{50,\alpha}$, $V_{50,\beta}$, $t_{50,\alpha}$ and $t_{50,\beta}$ could be obtained.

Again, to evaluate the validity of fitting with two instead of one *erf*-function, AIC was used.

Prediction of firing threshold and refractory period based on diameter of nerve fibres

In the normal nerve there exists an empirical inverse relation between the diameter of the nerve fibres and both the extracellular firing threshold [17, 18] and the refractory period [19]. This relation can be exploited to assess qualities of the regenerated nerve fibres. Based on the observed mean diameter in the experimental groups and the mean diameter and mean voltage threshold of the control group the predicted values of the mean voltage threshold in the experimental group can be calculated using equation 1

$$V_{50,g,predicted} = \frac{V_{50,c} * d_{Fmax,c}}{d_{Fmax,g}} \qquad \text{(eq. 1)}$$

The predicted value of the mean refractory period (eq. 2), as well as the predicted mean thresholds and refractory periods of the Aα- and Aβ-fibre populations can be calculated with the same equations, by substituting the appropriate values.

$$t_{50,g,predicted} = \frac{t_{50,c} * d_{Fmax,c}}{d_{Fmax,g}} \qquad \text{(eq. 2)}$$

Prediction of Q based on number and diameter of nerve fibres

The charge, Q_{max} is proportional to the product of the number of excitable nerve fibres and the square of their mean diameter [cf. 14, 20]. Hence the predicted value of Q_{max} can be calculated with equation 3. Predicted values of Q_{max} of the Aα- and Aβ-fibre populations can be calculated with the same equation, by substituting the appropriate values.

$$Q_{max,g,predicted} = \frac{Q_{max,c} * N_g * d^2_{Fmax,g}}{N_c * d^2_{Fmax,c}} \qquad \text{(eq. 3)}$$

Comparison of the experimentally measured values of these parameters to the predicted values will yield some insight in the quality of regeneration (see discussion).

Statistical evaluation

The means of all parameters were shown with standard deviations (mean ± sd). Student's t-tests were applied to the means to compare the control and autograft values with the synthetic nerve graft values. If a statistical significant difference was found with two or more of the synthetic nerve graft values, a one-way ANOVA was applied to the means, followed by Tukey's least significant differences multiple comparisons test to investigate differences between the groups. Fisher exact tests were applied to the electrophysiological response rates. Kolmogorov-Smirnow tests were applied to the different nerves and to the different samples per nerve for comparison of size distributions [21, 22]. Paired Student's t-tests were used to compare calculated and predicted values of V_{50}, t_{50} and Q_{max}. The SPSS statistical program, version 11.0, and Origin, version 5.0, were used to calculate means and standard deviations, and to perform statistical analysis. P-values of less than 0.05 or, in case of the electrophysiological-morfometrical relations 0.05 and 0.10, were regarded as significant.

Results

Upon macroscopic inspection, both the *non porous* and the *porous* grafts had partially degraded. In all cases that received synthetic nerve grafts, a gel-like shell that surrounded the tissue bridge at the implantation site was visible. A tissue bridge was present in all rats in both synthetic nerve graft groups.

All autografted nerves exhibited a patent graft at 12 weeks after surgery. The grafted part was slightly thinner. The distal nerves proved to be firm and shiny white, without the softening one would expect after Wallerian degeneration [23]. Some connective tissue was present around the coaptation sites.

Midgraft morphology

The midgraft morphology of *non porous* and *porous* nerve grafts was similar. The cross-sections of the regenerated structure had an oval shape and demonstrated a centrally located nerve-like structure which was surrounded by a cellular outer layer, areas of trabecular structures and a collagen-rich encapsulating structure (fig. 2).

In both types of grafts the centrally located nerve-like structure consisted of myelinated nerve fibres, cell nuclei (at least some of them Schwann cell nuclei since myelin was present around the nerve fibres) and amorphous extracellular matrix. This area was surrounded by a cell-rich layer of circularly oriented fusiform cells (presumably fibroblasts) embedded in an extracellular matrix rich in collagen. Thin walled blood vessels and capillaries were observed throughout the cross section, though most of the larger vessels were located in the outer

Figure 2: Light microscopic midgraft cross-sections of regenerating nerves

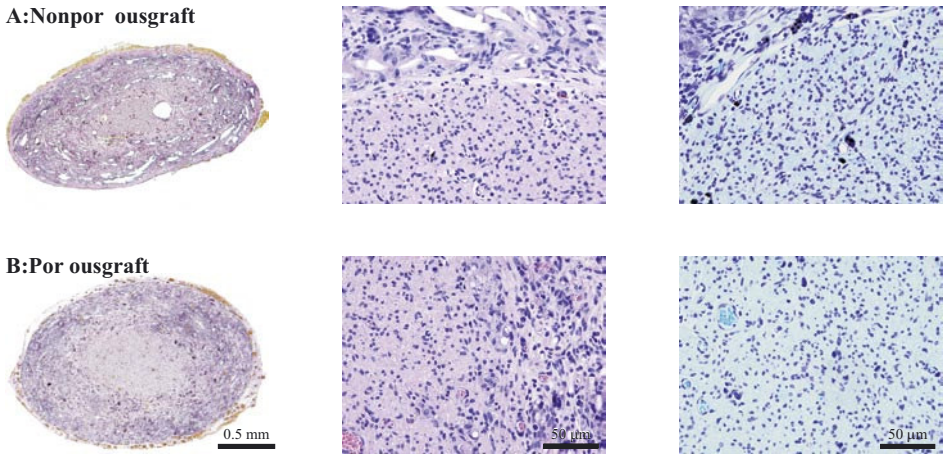

Transverse (4 µm) cross-sections of midgraft sciatic nerves, immersion fixed after electrophysiological evaluation, and stained with haematoxylin/eosin, according to the method of Klüver-Barrera to clearly identify myelin sheaths [12], and according to the method of Verhoef van Gieson to clearly identify collagen [13] are depicted. In all figures, the left panel represents the Verhoef van Gieson stained nerve section as a whole. Elastic fibres are stained black, nuclei blue and cytoplasm yellow/brown. The middle panel represents an enlarged sample of the haematoxylin/eosin nerve section and demonstrates the morphology of the nerve in detail. The right panel depicts an enlarged sample of the nerve section, stained according to the method of Klüver-Barrera, in which the myelin sheath is deep blue and is therefore more pronounced.
A. Cross-section of a *non porous* nerve graft. B. Cross-section of a *porous* nerve graft.

layer. Throughout this outer layer fragments of smooth material surrounded by rings of large round cells could be distinguished. The smooth material appeared to be fragments of bio - material, being broken down by the round large cells. The cell-rich layer was surrounded by areas of trabecular structures, which seemed to be the remnants of the tubal wall. All grafts were encapsulated by a continuous structure, which was rich in collagen. This encapsulating structure also contained fragments of smooth material, which remarkably had round large cells in the center, as though breakdown of the biomaterial took place from the inside of the fragments of biomaterial.

Morphology of the peroneus

Light microscopy of sections demonstrated that regenerating peroneal nerves were vascular - ized and enclosed in a connective-tissue sheath. They contained many myelinated axons, abundant endoneurial connective tissue and blood vessels (fig. 3, left column). The myelin sheaths of the nerve fibres in grafted nerves were obviously thin in comparison to those in controls. The nerve fibres in autograft peroneal nerves, and sporadically in synthetic nerve grafted nerves, were frequently bundled within areas of size comparable to the cross-section of single myelinated fibres in control nerves, suggesting regeneration of several nerve fibres through single Schwann cell basal laminar scaffolds that persisted after Wallerian degenera - tion of the original myelinated nerve fibres [24]. The fibre diameter frequency distributions (fig. 3, middle and right column) demonstrated that in regenerating peroneal nerves fibre diameters shifted to smaller sizes.

Figure 3: Light microscopic cross-sections and frequency distributions of control and graft peroneal nerves

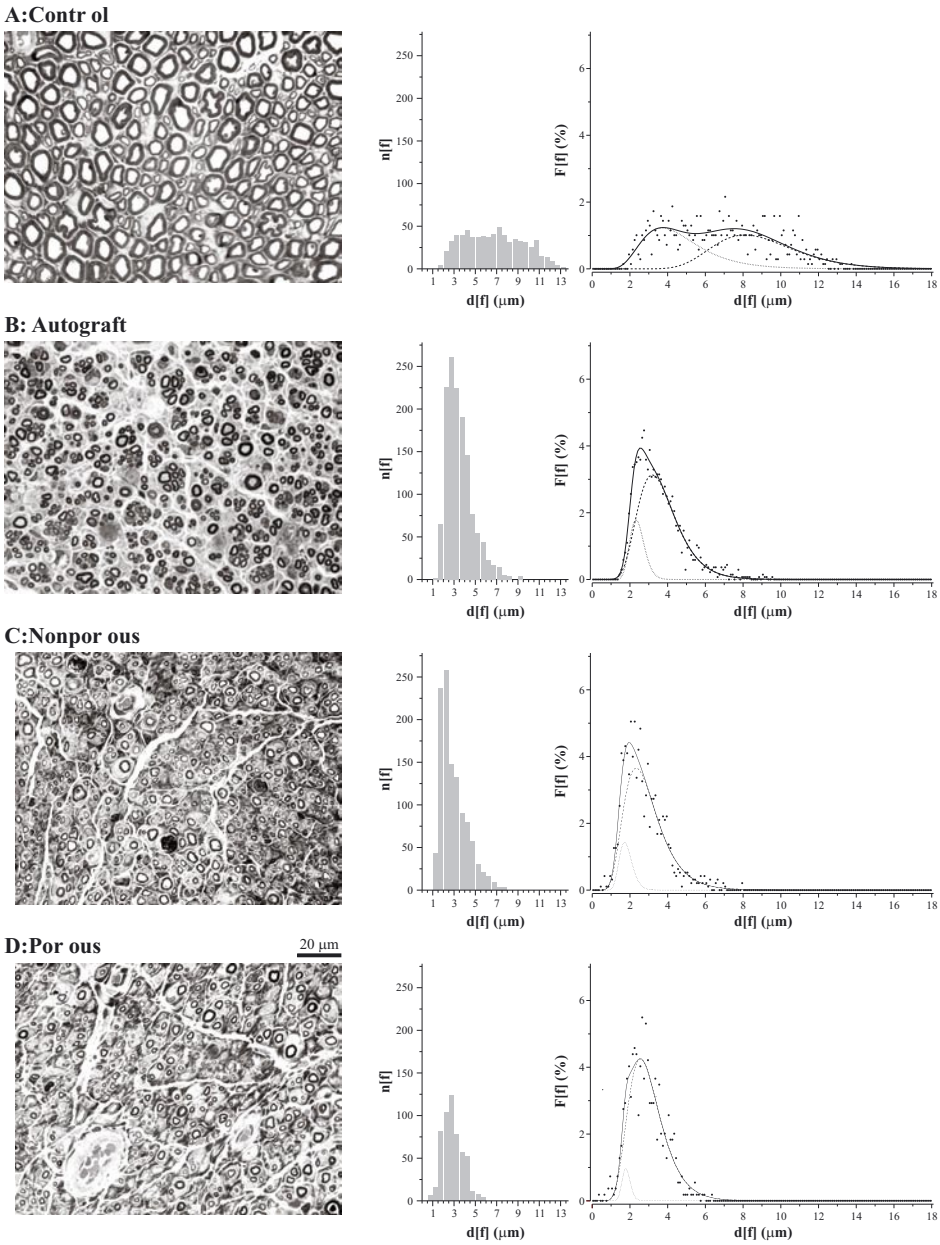

Transverse semi-thin (1 µm) cross-sections of peroneal nerves, immersion fixed after electrophysiological evaluation, and stained with a 1% toluidine blue / 1% borax solution [16] are depicted. In all figures, the left panel represents the nerve section as a whole, whereas in the middle panel an enlarged sample of this nerve section (square) demonstrates the morphology of the nerve in detail. The right panel depicts typical examples of the frequency distributions of fibre diameters of control, autografted, *non porous*, and *porous* grafted peroneal nerves. In each graph, diameters of the nerve fibres were distributed into 28 classes of 0.5 µm each, and plotted against the fibre diameter class frequency. The dots represent the calculated fibre diameter class frequency per fibre diameter class, the straight line represents the fit of total curve, the dotted line represents the Aβ-fibre population, and the dashed line represents the Aα-fibre population.

Figure 4: Morphometric analysis

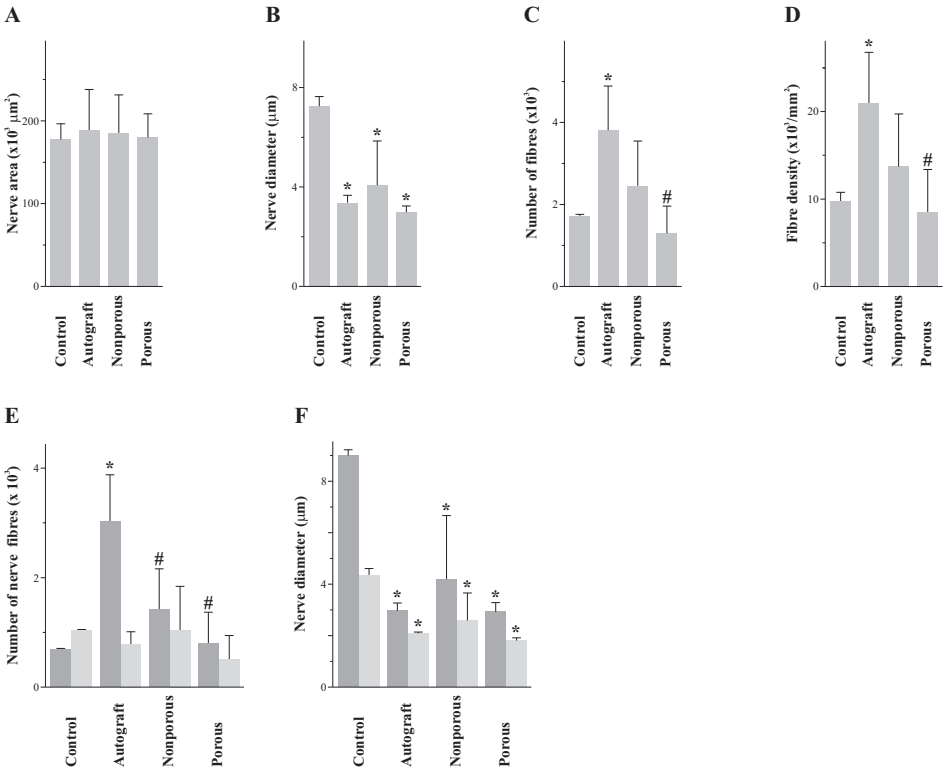

Morphometric data of the control, autografted and synthetic grafted nerves are depicted. A. The total surface of the nerve cross section (nerve area), B. the nerve fibre diameter, C. the number of nerve fibres, D. the nerve fibre density, E. the number of nerve fibres for the Aα- and Aβ-fibre population separately, and F. the nerve fibre diameter for the Aα- and Aβ-fibre population separately. Data are represented as mean (± sd). (*) Different compared to control nerves. (#) Different compared to autograft nerves.

All nerve areas were of comparable size (fig. 4A), and the fibre diameters of grafted nerves were halved compared to controls (fig. 4B). The total number and the density of nerve fibres were doubled after autografting, and remained unchanged in synthethic grafted nerves (fig. 4C and D). In *porous*, but not in *non porous* nerve grafts the number of nerve fibres and the nerve fibre density was smaller compared to autografts.

Kolmogorov-Smirnow tests revealed a homogeneous fibre size distribution throughout control nerves, and a homogeneous fibre size distribution within individual control nerves. In the regenerating nerves, both heterogeneity and homogeneity in fibre size distributions between nerves, and within individual nerves, were encountered.

The sum of two lognormal distributions could satisfactorily be fitted to the fibre diameter distributions of both control and graft peroneal nerves (fig. 3, right column). In all examined nerves, the AIC was determined and shown to be smaller ($p<10^{-4}$) for two populations compared to one, indicating that the fibre diameter distribution could be more aptly described by the sum of two lognormal distributions rather than by one lognormal distribution.

Table 2: Muscle CSA and reorganization of type I and type II musclefibres after reinnervation

Tibial muscle	muscle CSA (x 10^6 µm^2)	number of type I muscle fibres	type I muscle fibre CSA (µm^2)	number of type II muscle fibres	type II muscle fibre CSA (µm^2)
Control	38.1 ± 6.5	170 ± 97	1410 ± 256	7774 ± 1154	4883 ± 587
Autograft	22.6 ± 6.5*	314 ± 209	2093 ± 623	6113 ± 1866	3636 ± 721*
Non porous graft	27.4 ± 8.5	164 ± 119	1894 ± 478	7961 ± 2288	3485 ± 921*
Porous graft	19.2 ± 3.4*	20 ± 4*#	1294 ± 275	7541 ± 1088	2620 ± 673*
Gastrocnemic muscle	muscle CSA (x 10^6 µm^2)	number of type I muscle fibres	type I muscle fibre CSA (µm^2)	number of type II muscle fibres	type II muscle fibre CSA (µm^2)
Control	73.8 ± 6.4	1256 ± 462	2322 ± 405	11079 ± 1777	6474 ± 520
Autograft	43.2 ± 8.7*	635 ± 397*	3002 ± 703	11459 ± 2720	3700 ± 661*
Non porous graft	41.1 ± 13.5*	639 ± 327	2431 ± 1133	9939 ± 2065	4191 ± 1390*
Porous graft	32.6 ± 8.7*	451 ± 248*	1427 ± 458*#	10945 ± 1895	3007 ± 974*

Muscle CSA, type I and type II muscle fibre number and CSA in muscles innervated by control, autografted, *non porous*, and *porous* nerve grafted sciatic nerves. Data are represented as mean (± sd). (*) Different compared to control muscles. (#) Different compared to autograft muscles.

In control peroneal nerves, the number of Aβ-fibres was somewhat higher compared to the number of Aα-fibres (fig. 4E). In regenerated nerves it was the other way round: the number of Aα-fibres was higher than the number of Aβ-fibres. In autograft peroneal nerves, the number of Aα-fibres increased fivefold, while in the synthetic grafted nerves the number of Aα-fibres remained equal (*porous* grafts) or doubled (*non porous* grafts). In all regenerated nerves, the number of Aβ-fibres remained unchanged. The diameter of Aα-fibres decreased three times and the diameter of Aβ-fibres halved in all experimental nerve fibres (fig. 4F).

Morphology of the muscles

The muscle CSA diminished to half its size in grafted muscles (table 2).

The type II muscle fibre CSA also declined to half its size in graft muscles, which was not surprising, regarding the predominance of type II muscle fibres. The number of type II muscle fibres remained equal. An overall impression of the changes in type I muscle fibres is that the opposite took place. Type I muscle fibre CSA remained equal in graft muscles, while the number of type I muscle fibres declined. The number of type I muscle fibres in tibial muscles was very small, and therefore varied considerably.

Electrophysiology

Electrophysiological response rates in the four groups ranged from 67 to 100%, which was not statistically different (figure 5B). Q_{max} was highest in control nerves, lower in autografted nerves, and lowest in the synthetic grafted nerves (fig. 5C and D). Q_{max} of synthetic grafted nerves did not demonstrate differences between the groups, and the mean value of Q_{max} derived from the interpulse time-recruitment curves was not different from that obtained from the stimulus-recruitment curves. The MCV was three to four times slower in auto- and

Figure 5: Recordings of compound nerve action currents

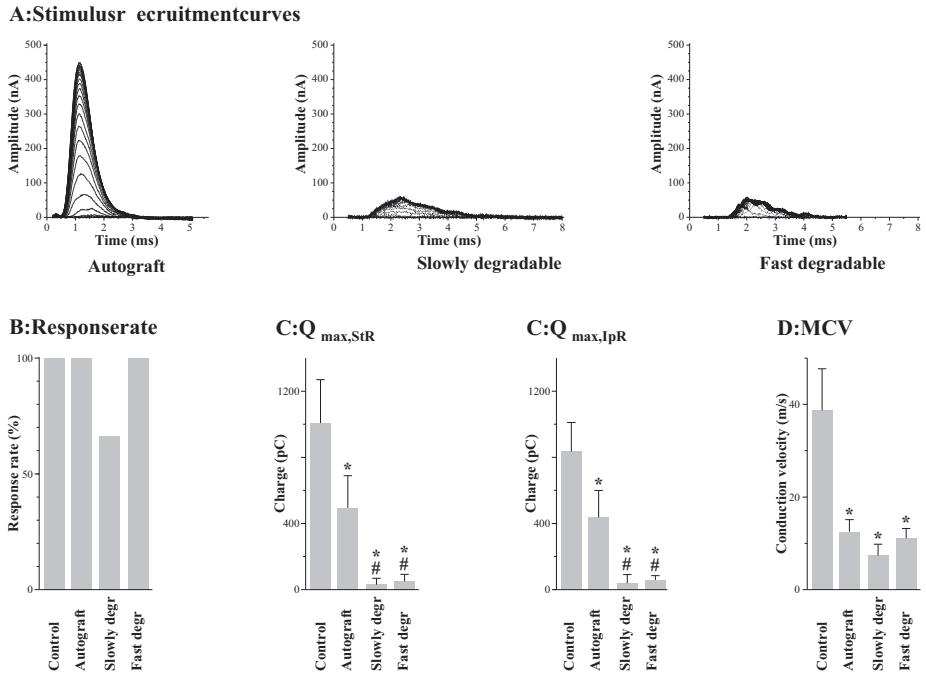

A. Examples of the time courses of compound action currents as a function of stimulus voltage of synthetic grafted sciatic nerves. In each graph, the curves from bottom to top represent compound action currents, evoked by increasing stimulus voltages. Stimulus artifacts were erased. Due to the virtual cathode effect [42] the onset of the current moves closer to the stimulus artifact upon increasing the stimuli. The amplitude of the monophasic action current gradually increased in response to increasing stimulus voltages, until a maximum amplitude was reached. The voltage stimulus necessary to attain the maximum action current amounted to approximately 4 V in control nerves and 10 V in grafted nerves.
B. Electrophysiological response rate.
C. Q_{max} derived from stimulus-recruitment data.
D. Q_{max} derived from interpulse time-recruitment data.
E. MCV.
Data are represented as mean ± sd. (*) Different compared to control nerves. (#) Different compared to autograft nerves.

synthetic grafted nerves, and the differences between grafted nerves were not significant (fig. 5E).

The stimulus-recruitment curves (fig. 6A), corresponding to the figures representing the monophasic action currents (fig. 5A), demonstrated that in the *non porous* grafts there was a tendency that the contribution of the Aα- and the Aβ-fibres to Q_{max} was comparable, but that in *porous* grafted nerves the contribution of the Aα-fibres to Q_{max} was larger than that of the Aβ-fibres. However, this did not lead to significant differences between $Q_{max,\alpha}$ and $Q_{max,\beta}$ in the synthetic nerve graft groups (fig. 6B).

The mean voltage threshold (V_{50}) was higher in grafted nerves in comparison to control nerves. The V_{50} in *non porous* nerves increased only moderately, and was significantly smaller in comparison to autografted nerves (fig. 6C). Both $V_{50,\alpha}$ and $V_{50,\beta}$ doubled in all regenerating nerves, with the exception of the values of $V_{50,\alpha}$ and $V_{50,\beta}$ in the *non porous* group, which were comparable to those in control nerves (fig. 6D). In all regenerating nerves, the mean

Figure 6: Stimulus-recruitment curves

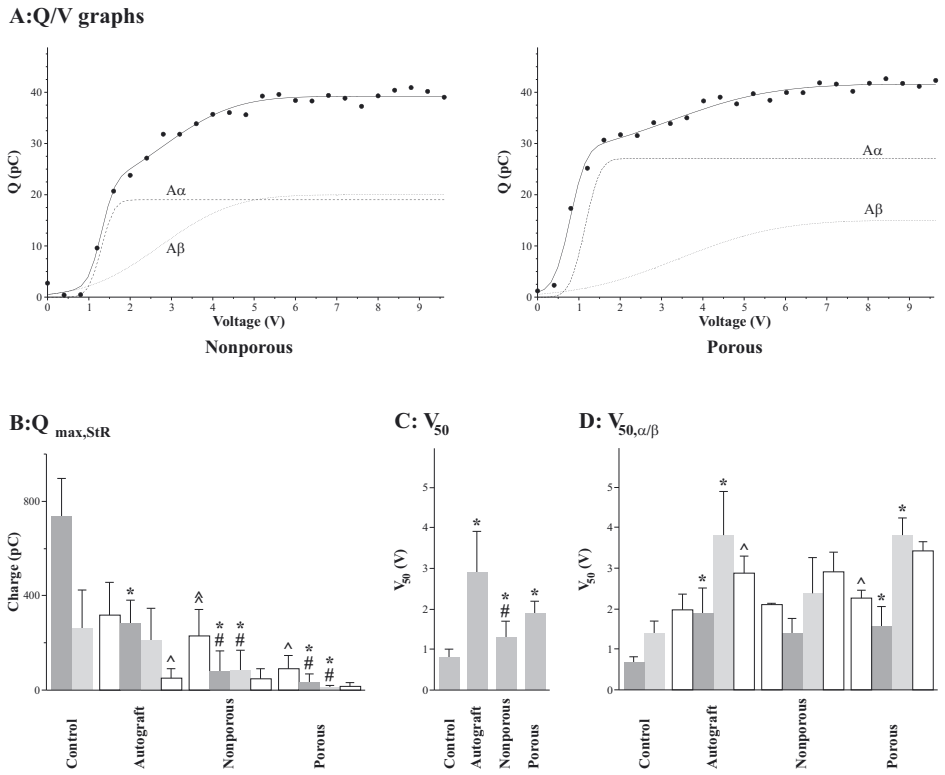

A: Stimulus-recruitment graphs corresponding to the examples depicted in figure 5A. Solid circles represent data points. Continuous lines represent the fitted curves. The AIC proved to be smaller ($p<10^{-4}$) for two populations compared to one. B. The $Q_{max,\alpha}$ (dark grey) and $Q_{max,\beta}$ (light grey) of control, autografted, *non porous* and *porous* grafted nerves derived from the stimulus-recruitment data. The predicted values of $Q_{max,\alpha}$ and $Q_{max,\beta}$ are represented by unfilled bars. C. Mean voltage threshold (V_{50}) of control, autografted, and synthetic grafted sciatic nerves. D. Mean firing threshold for the Aα- and Aβ-fibres separately ($V_{50,\alpha}$ and $V_{50,\beta}$) of control, autografted, and synthetic grafted sciatic nerves. The predicted values of $V_{50,\alpha}$ and $V_{50,\beta}$ are represented by unfilled bars. Data are represented as mean (± sd). (*) Different compared to control group. (#) Different compared to autograft group. (^) Different compared to predicted values, $p<0.05$. (^^) Different compared to predicted values, $p<0.10$.

threshold voltage of the Aα-fibres ($V_{50,\alpha}$) was approximately half the value of $V_{50,\beta}$, as in the control nerves.

The interpulse time-recruitment curves, corresponding to those nerves of which the stimulus-recruitment curves were depicted in figure 6A, demonstrated again that the contribution of the Aα-fibres to Q_{max} was larger than the contribution of the Aβ-fibres (fig. 7A), as in control and autografted nerves (fig 7B). Likewise, between synthetic nerve grafts no differences in $Q_{max,\alpha}$ or $Q_{max,\beta}$ were encountered (fig 7B).

The response in the grafted nerves was characterized by a longer mean refractory period (t_{50}) compared to control nerves (fig. 7C). The refractory period doubled in autografted and *porous* grafted nerves, but quadrupled in *non porous* grafted nerves. The value of $t_{50,\alpha}$ demonstrated a similar pattern (fig. 7D). The value of $t_{50,\beta}$ approximately doubled in the autografted, tripled in

Figure 7: Interpulse time-recruitment curves

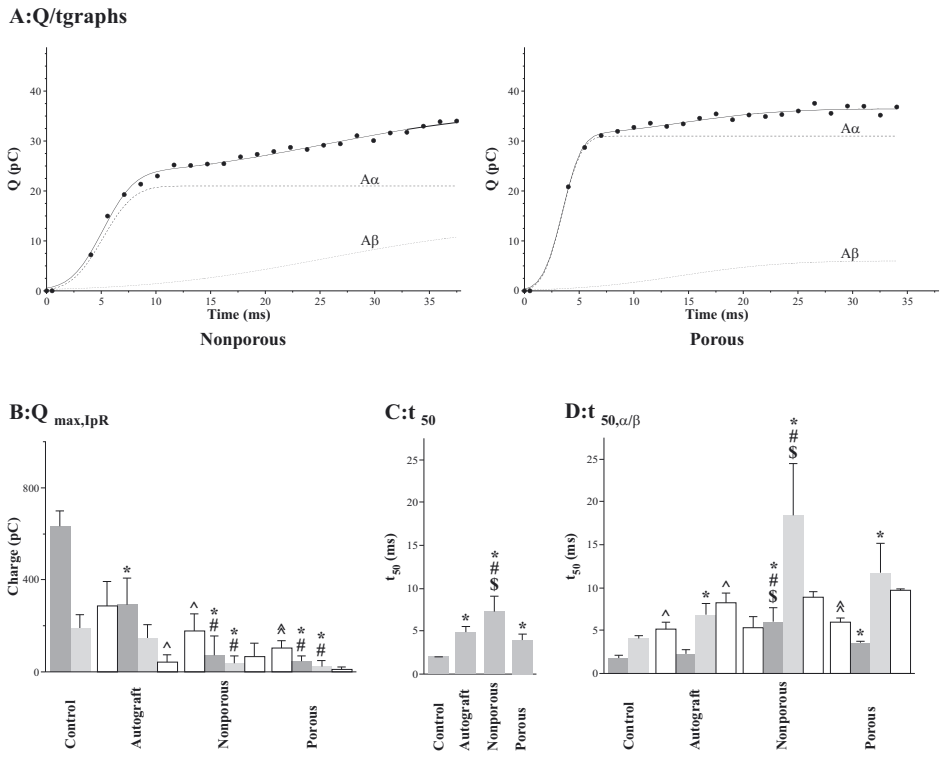

A: Interpulse time-recruitment graphs corresponding to the examples depicted in figure 5A. Solid circles represent data points. Continuous lines represent the fitted curves. The theoretical dataset (Δt = 0, Q = 0) was added to the data. The AIC proved to be smaller ($p<10^{-4}$) for two populations compared to one. B. The $Q_{max,\alpha}$ (black) and $Q_{max,\beta}$ (white) of control, autografted, *non porous* and *porous* grafted nerves derived from the interpulse time-recruitment data. The predicted values of $Q_{max,\alpha}$ and $Q_{max,\beta}$ are represented by unfilled bars. C. Mean refractory period (t_{50}) of control, autografted, and synthetic grafted sciatic nerves. D. Mean refractory period for the Aα- and Aβ-fibres separately ($t_{50,\alpha}$ and $t_{50,\beta}$) of control, autografted, and synthetic grafted sciatic nerves. The predicted values of $t_{50,\alpha}$ and $t_{50,\beta}$ are represented by unfilled bars. Data are represented as mean (± sd). (*) Different compared to control group. (#) Different compared to autograft group. ($) Different compared to *fast degradable* and *slowly degradable* group. (^) Different compared to predicted values, $p<0.05$. (^^) Different compared to predicted values, $p<0.10$.

the *porous* group, and quadrupled in the *non porous* group. The mean refractory period of the Aα-fibres ($t_{50,\alpha}$) was approximately one third of $t_{50,\beta}$, both in control and in grafted nerves.

Relation of morphometric and electrophysiological data

Both the measured V_{50} and t_{50} in the Aα-fibres were lower than predicted in the *porous*, but not in the *non porous* nerve graft group (fig. 6 and 7D). In the Aβ-fibres, the measured V_{50} and t_{50} were according to predictions.

In both *porous* and *non porous* grafted nerves, the measured charge in the Aα-fibres was lower than predicted (fig. 6 and 7B). The measured charge in the Aβ-fibres was just as was predicted based on morphological changes.

Discussion

Twelve weeks after surgery, the morphometrical parameters of the peroneal nerves and the gastrocnemic and tibial muscles were similar if not equal in the synthetic nerve grafted rats. Electrophysiologically, however, a distinction could be made between *porous* and *non porous* grafts. The refractory period lenghtened in all regenerated nerves, but $t_{50,\alpha}$ and $t_{50,\beta}$ were significantly shorter in *porous* grafted nerves compared to *non porous* grafted nerves.

In contrast $V_{50,\alpha}$ en $V_{50,\beta}$ were increased in *porous* grafted nerves, whereas these thresholds remained equal in *non porous* grafted nerves, both compared to unoperated nerves.

The closer to normal the refractory period is, the better the regenerated axon will be able to pass all axon potentials generated by the motorneuron. A moderate increase of the firing threshold along the axon is of little influence on the capacity of the axon to transmit action potentials, indeed an increase of the firing threshold will decrease the probability of the generation of spontaneous action potentials along the axon. For these reasons we deem the refractory period to be the most important parameter. The firing threshold is not as influential on the function of the axon, though its value should not be lower than normal, which would result in hyperexcitability and neuropathic pain [25, 26, 27]. Given the tendency of injured and regenerating axons to spontaneous firing [28, 29] a higher than normal threshold (within limits) might even be preferable. Based on this line of reasoning the *porous* nerve grafts, possessed of the shorter refractory periods and the higher firing thresholds are preferable.

In order to interpret the changes in especially t_{50}, but also in $V_{50,}$ the factors that determine the value of those electrophysiological parameters were considered. Since an empirical inverse relation exists between the diameter of the nerve fibres and both the extracellular firing threshold and the refractory period, measured values of V_{50} and t_{50} were compared to predicted values. Equality of the measured and predicted values indicates that no other changes but changes of diameter have occurred, while inequality indicates that additionally other changes must have occurred. The most obvious and best documented of those are changes in the expression of ion channels at or near the Ranvier nodes [30-34].

In *porous* nerve grafts a faster repolarization and a lower voltage threshold than predicted was observed in the Aα-fibres, indicating that compensatory mechanisms were active and thus that presumably the ion channel composition changed. Upregulation of the $Na_{v1.3}$ channels would lead to a shorter refractory period [31, 35]. A shorter refractory period can also be caused by a faster potassium efflux, which can be effectuated by an increase in the number of channels in the membrane or by a more effective closing of the channels [36]. Such an upregulation was described before in spinal sensory neurons after axotomy [37] and in crushed nerves [39]. Although the measured V_{50} in *porous* nerve grafts was higher, the value was still lower than predicted. This can be due to a downregulation

of $Na_{v1.8}$ and $Na_{v1.9}$ channels, as demonstrated before to occur after axotomy [28, 38]. These assumptions can easily be verified by immunohistochemically staining the ion channels in the nerve fibre membrane. It was demonstrated before that the ion channel composition changed indeed after peripheral nerve injury and subsequent repair [37].

Thus, empirically the presence of pores can be related to a shorter refractory period, which hypothetically can be related to a compensatory change in ion channel composition of the axonal membrane. However, it is interesting to consider how the distribution of different kinds of ion channels over the (para)nodal regions can be influenced by the presence of pores in the synthetic nerve grafts. It is well known that plasticity of Na+ channel gene expression occurs in the normal nervous system [28], and also that the sodium channel expression changes continuously in the weeks after axotomy [31, 34, 28, 29, 38].

In this paper, it is hypothesized that the capacity to adapt the ion channel composition towards the situation that the nerve fibres have a refractory period and threshold voltage alike the unoperated situation, which is considered the most favorable situation, increases upon maturation of the nerve fibres.

It is further hypothesized here that porosity of the nerve graft positively influences maturation of the nerve fibres by speeding up the formation of a tissue bridge. We demonstrated before that the diameter of the tissue bridge was convincingly larger in porous vs. non porous nerve grafts (chapter 4, this thesis). Now, it is proposed that pores positively influence the size of the tissue bridge by allowing inward diffusion of growth factors and extracellular matrix proteins [1], and outward diffusion of waste products. Such assumptions were also made by others [39]. We presume that TMC at least partially degraded within the survival period of 12 weeks, based on results on the *in vitro* and *in vivo* degradation of TMC [10, 40]. It is thus very likely that the inner layer of the *non porous* nerve grafts became porous during this survival period. Possibly, the tissue bridge was formed or the quality of the tissue bridge improved only after the graft became porous, thereby causing a delay in maturation of the nerve fibres in the *non porous* nerve grafts.

The formation of a tissue bridge can hypothetically also be influenced by the microgeometry of the inner layer of synthetic nerve grafts [41, 42]. The inner layer of the *porous* nerve graft is somewhat rough, in contrast to the smooth inner layer of the *non porous* nerve graft (fig. 1). A rough inner layer seems more favorable for the formation of a tissue bridge, and may have contributed to a prompt formation of a tissue bridge.

Besides all this, it is remarkable that the number of nerve fibres in the *porous* nerve graft was lower in comparison to autografted nerves, in contrast to the number of fibres in *non porous* nerve grafts which demonstrated an equal number of fibres. It can be presumed that the pruning of an overflow of regenerating nerve fibres is still going on [43] and this corresponds very well to a delay in the maturation of regenerating nerve fibres.

In conclusion, *porous* nerve grafts are favoured over *non porous* nerve grafts, because the refractory period is shorter and because it is likely that the nerve fibres were able to compensate for their smaller diameter by changing their ion channel composition.

References

1. Kim DH, Connolly SE, Zhao S, Beuerman RW, Voorhies RM, Kline DG. Comparison of macropore, semipermeable, and nonpermeable collagen conduits in nerve repair. J Reconstr Microsurg 1993;9:415-20.
2. Rutkowski GE, Heath CA. Development of a Bioartificial Nerve Graft. II. Nerve Regeneration in Vitro. Biotechnol Prog 2002;18:373-9.
3. Jenq CB, Coggeshall RE. Nerve regeneration through holey silicone tubes. Brain Res 1985;361:233-41.
4. Jenq CB, Jenq LL, Coggeshall RE. Nerve regeneration changes with filters of different pore size. Exp Neurol 1987;97:662-71.
5. Jenq CB, Coggeshall RE. Permeable tubes increase the length of the gap that regenerating axons can span. Brain Res 1987;408:239-42.
6. Knoops B, Hurtado H, van den Bosch de Aguilar P. Rat sciatic nerve regeneration within an acrylic semipermeable tube and comparison with a silicone impermeable material. J. Neuropathol. Exp. Neurol. 1990;49:438-448.
7. Chamberlain LJ, Yannas IV, Arrizabalaga A, Hsu HP, Norregaard TV, Spector M. Early peripheral nerve healing in collagen and silicone tube implants: myofibroblasts and the cellular response. Biomaterials 1998;19:1393-403.
8. Keeley RD, Nguyen KD, Stephanides MJ, Padilla J, Rosen JM. The artificial nerve graft: a comparison of blended elastomer-hydrogel with polyglycolic acid conduits. J Reconstr Microsurg 1991;7:93-100.
9. Pego AP, Poot AA, Grijpma DW, Feijen J. Biodegradable elastomeric scaffolds for tissue engineer - ing. Proceedings of the 4th international symposium on frontiers in biomedical polymers. Wil - liamsburg, Virginia, USA, 2001:54.
10. Pego AP. Biodegradable polymers based on trimethylene carbonate for tissue engineering ap - plications. Polymer Chemistry and Biomaterials. Enschede: University of Twente, 2002:291.
11. Marani E. A method for orienting cryostat sections for three-dimensional reconstructions. Stain Technol. 1978;53:265-268.
12. Kluver H, Barrera E. A method for the combined staining of cells and fibers in the nervous system. Neuropath Exp Neur 1953;12:400-403.
13. Bancroft JD, Gamble M. Theory and practice of histological techniques. London: Churchill Living - stone, 2002.
14. Vleggeert-Lankamp CLAM, Van den Berg RJ, Feirabend HKP, Lakke EAJF, Malessy MJA, Thomeer RTWM. Electrophysiology and morphometry of the Aalpha and Abeta fibre populations in the normal and regenerating rat sciatic nerve. Experimental Neurology 2004;187:337-349.
15. Vleggeert-Lankamp CLAM, Ruiter de GCW, Wolfs JFC, Pego AP, Feirabend HKP, Lakke EAJF, Malessy MJA. Type grouping in skeletal muscles after experimental reinnervation: another explanation. European Journal of Neuroscience 2005;21:1249-1256.
16. Feirabend HKP, Choufoer H, Ploeger S. Preservation and staining of myelinated nerve fibers. Meth - ods 1998;15:123-31.
17. Blair EA, Erlanger J. A comparison of the characteristics of axons through their individual electrical responses. Am J Physiol 1933;106:524-564.
18. Jack JJB, Noble D, Tsien RW. Electric current flow in excitable cells: Oxford University Press, 1983.
19. Paintal AS. The influence of diameter of medullated nerve fibres of cats on the rising and falling phases of the spike and its recovery. J Physiol 1966;184:791-811.

20. Rushton WAH. A theory of the effects of fiber size in medullated nerve. J Physiology 1951;115:101-122.
21. Kolmogorov A. Confidence limits for an unknown distribution function. Ann. Meth. Statist. 1941;12:461-463.
22. Smirnow NV. Table for estimating the goodness of fit of empirical distributions. Ann. Meth. Statist. 1948;19:279-281.
23. Seckel BR, Chiu TH, Nyilas E, Sidman RL. Nerve regeneration through synthetic biodegradable nerve guides: regulation by the target organ. Plast Reconstr Surg 1984;74:173-181.
24. MacKinnon SE, Hudson AR, Hunter DA. Histologic assessment of nerve regeneration in the rat. Plast Reconstr Surg 1985;75:384-388.
25. Devor M, Govrin-Lippmann R, Angelides K. Na+ channel immunolocalization in peripheral mammalian axons and changes following nerve injury and neuroma formation. J Neurosci 1993;13:1976-92.
26. Waxman SG, Cummins TR, Black JA, Dib-Hajj S. Diverse functions and dynamic expression of neuronal sodium channels. Novartis Found Symposium, 2002:34-51, discussion 51-60.
27. Abdulla FA, Smith PA. Changes in Na+ channel currents of rat dorsal root ganglion neurons following axotomy and axotomy-induced autotomy. J Neurophys 2002;88:2518-2529.
28. Burchiel KJ. Spontaneous impulse generation in normal and denervated dorsal root ganglia: sensitivity to alpha-adrenergic stimulation and hypoxia. Exp Neurol 1984; 85: 257-272.
29. Lisney SJ, Devor M. Afterdischarge and interactions among fibres in damaged peripheral nerve in the rat. Brain Res 1987; 415: 122-136.
30. Querfurth HW, Armstrong R, Herndon RM. Sodium channels in normal and regenerated feline ventral spinal roots. J Neurosci 1987;7:1705-1716.
31. Cummins TR, Waxman SG. Downregulation of tetrodotoxin-resistant sodium currents and up regulation of a rapidly repriming tetrodotoxin-sensitive sodium current in small spinal sensory neurons after nerve injury. J Neurosci 1997;17:3503-14.
32. Everill B, Kocsis JD. Reduction in potassium currents in identified cutaneous afferent dorsal root ganglion neurons after axotomy. J Neurophysiol 1999;82:700-8.
33. Baccei ML, Kocsis JD. Voltage-gated calcium currents in axotomized adult rat cutaneous afferent neurons. J Neurophysiol 2000;83:2227-38.
34. Lancaster E, Weinreich D. Sodium currents in vagotomized primary afferent neurones of the rat. J Physiol 2001;536:445-458.
35. Waxman SG. Transcriptional channelopathies: an emerging class of disorders. Nat Rev Neurosci 2001;2:652-9.
36. Yellen G. The voltage-gated potassium channels and their relatives. Nature 2002;419:35-42.
37. Wolfs JFC, Vleggeert-Lankamp CLAM, Lakke EAJF, Thomeer RTWM. Ion channel redistribution over time in crushed rat sciatic nerve. Soc Neurosci Abstr, 2003.
38. Flake NM, Lancaster E, Weinreich D, Gold MS. Absence of an association between axotomy-induced changes in sodium currents and excitability in DRG neurons from the adult rat. Pain 2004;109:471-480.
39. Belkas JS, Munro CA, Shoichet MS, Midha R. Peripheral nerve regeneration through a synthetic hydrogel nerve tube. Rest Neur Neurosci 2005;23:19-29.
40. Pego AP, Poot AA, Grijpma DW, Feijen J. Copolymers of trimethylene carbonate and epsilon-caprolactone for porous nerve guides: synthesis and properties. J Biomater Sci Polym Ed 2001;12:35-53.
41. Aebischer P, Guenard V, Valentini RF. The morphology of regenerating peripheral nerves is modulated by the surface microgeometry of polymeric guidance channels. Brain Res 1990;531:211-8.

42. Guenard V, Valentini RF, Aebischer P. Influence of surface texture of polymeric sheets on peripheral nerve regeneration in a two-compartment guidance system. Biomaterials 1991;12:259-63.
43. Witzel C, Rohde C, Brushart TM. Pathway sampling by regenerating peripheral axons. J Comp Neur 2005;485:183-190.
44. Krarup C, Horowitz SH, Dahl K. The influence of the stimulus on normal sural nerve conduction velocity: a study of the latency of activation. Muscle Nerve 1992;15:813-21.